

Mechanisms of Magma Generation Beneath Hawaii and Mid-Ocean Ridges: Uranium/Thorium and Samarium/Neodymium Isotopic Evidence

Kenneth W. W. Sims,* Donald J. DePaolo, Michael T. Murrell, W. Scott Baldrige, Steven J. Goldstein, David A. Clague

Measurements of uranium/thorium and samarium/neodymium isotopes and concentrations in a suite of Hawaiian basalts show that uranium/thorium fractionation varies systematically with samarium/neodymium fractionation and major-element composition; these correlations can be understood in terms of simple batch melting models with a garnet-bearing peridotite magma source and melt fractions of 0.25 to 6.5 percent. Mid-ocean ridge basalts shows a systematic but much different relation between uranium/thorium fractionation and samarium/neodymium fractionation, which, although broadly consistent with melting of a garnet-bearing peridotite source, requires a more complex melting model.

Measurements of $^{230}\text{Th}/^{232}\text{Th}$ and $^{238}\text{U}/^{232}\text{Th}$ isotopic ratios in basaltic lavas should, in principle, provide important information on the rate at which basaltic magmas form and are extracted from the upper mantle and on the extent of mantle melting required to produce basaltic melts (1). Uranium/thorium isotopic measurements on mid-ocean ridge basalts (MORBs) are enigmatic, however, in that unexpectedly large U/Th fractionations are observed (up to 35%), which seemingly indicate that MORBs represent very small melt fractions (<<1%) (2–4). Because other evidence indicates that larger melt fractions characterize the melting regime of MORBs (5 to 20%) (5, 6), there is some question about whether U/Th fractionation is related to melt fraction by crystal-melt partitioning or may instead be controlled by disequilibrium or secondary processes (7). To investigate the causes of U/Th fractionations during basalt petrogenesis, we made high-abundance sensitivity mass spectrometric measurements of U and Th isotopic ratios in a series of lavas from Hawaii that have trace-element and petrological characteristics indicating that they span a large range of melt fraction. To compare basalt petrogenesis in the mid-ocean ridge and Hawaiian Islands settings, we also analyzed a suite of MORBs from the Juan de Fuca and Gorda ridges, including both normal (N-MORB) and en-

riched (E-MORB) samples (3).

Numerous studies on lavas from the Hawaiian Islands have shown that, over the life-span of a volcano, the major- and trace-element chemistry of the erupted basalts varies significantly and systematically (8). To obtain young lavas with a range of compositions, we sampled historic or young and dated [$< 5 \times 10^3$ years ago (ka)] lavas from different Hawaiian volcanoes. Tholeiitic lavas were collected from Kilauea, Mauna Loa, and Loihi; alkalic lavas were collected from Loihi, Mauna Kea, Hualalai, and the South Arch; and basanitic lavas were collected from Haleakala and the South Arch. Collectively, this suite encompasses all four stages of Hawaiian volcano evolution. The compositional range of the Hawaiian samples is quantified in terms of normative hypersthene and nepheline content, the Mg-normalized Na content (5), and the inferred Sm/Nd fractionation (9–12).

One way in which inferred U/Th fractionations can be evaluated is by comparing them to the fractionation of another trace-element pair. We chose the Sm/Nd ratio because the Nd isotopic composition of the lavas provides information on the Sm/Nd ratio of the magma source (13–15), and the behavior of these elements during basalt petrogenesis is relatively well understood (12, 14). For both the Hawaiian and MORB data sets there is an excellent correlation between basalt type (tholeiite, alkali basalt, and basanite) and Sm/Nd fractionation (Fig. 1A and Table 1), as represented by the $\alpha_{\text{Sm/Nd}}$ value (9). For the Hawaiian samples there is a large range of Sm/Nd fractionation: The tholeiites are the least fractionated ($\alpha_{\text{Sm/Nd}} = 0.7$ to 0.8); the alkali basalts show an intermediate degree of fractionation ($\alpha_{\text{Sm/Nd}} = 0.6$ to 0.64); and the basanites are the most fractionated ($\alpha_{\text{Sm/Nd}} = 0.54$ to 0.61). The MORB samples, which are all tholeiitic, show less Sm/

Nd fractionation ($\alpha_{\text{Sm/Nd}} = 0.8$ to 0.9) than do the Hawaiian samples. There are good correlations between $\alpha_{\text{Sm/Nd}}$ and parameters $\text{Na}_{8,0}$ and silica saturation index (Fig. 1, B and C), petrologic parameters that are sensitive to melt fraction variations (16). All of

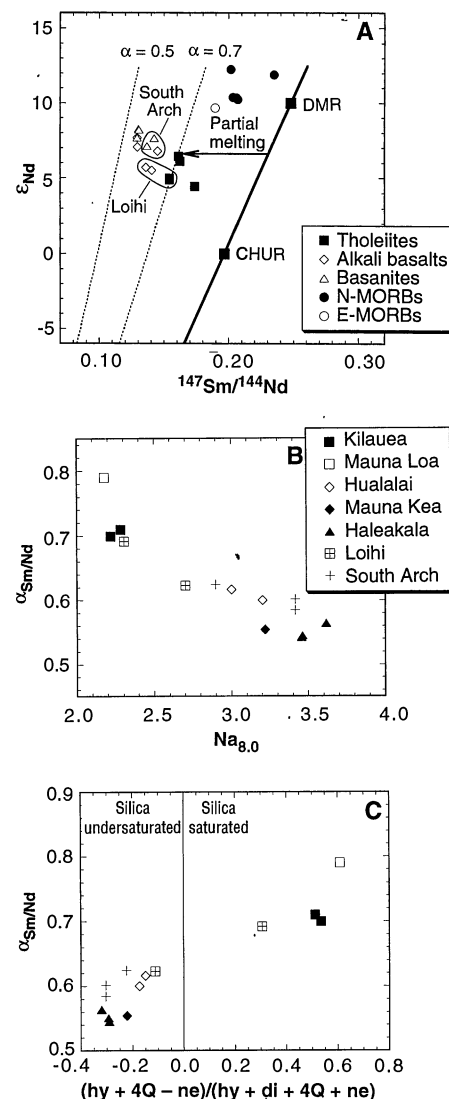


Fig. 1. (A) Plot of ϵ_{Nd} versus $^{147}\text{Sm}/^{144}\text{Nd}$ for Hawaiian basalts and MORBs. The solid dark line represents a 1.7-Ga isochron through the DMR, the average continental crust (not shown), and the CHUR (13). Partial melting (shown by the solid arrow) of any mixture of these three produces a magma with a lower $^{147}\text{Sm}/^{144}\text{Nd}$ ratio, but with the same ϵ_{Nd} value. The contours $\alpha = 0.5$ and 0.7 represent lines of equal $^{147}\text{Sm}/^{144}\text{Nd}$ fractionation relative to the mantle source with the same ϵ_{Nd} value (9, 13). The sizes of the data points are larger than the relative measurement error (2σ), based on in-run statistics (see Table 1). (B) Plot of $\alpha_{\text{Sm/Nd}}$ versus $\text{Na}_{8,0}$ for the Hawaiian basalts (5, 16). Major-element data for the Hawaiian basalts are available from the first author on request. (C) Plot of $\alpha_{\text{Sm/Nd}}$ versus $(\text{hy} + 4\text{Q} - \text{ne})/(\text{hy} + \text{di} + 4\text{Q} + \text{ne})$ for the Hawaiian basalts. The ratio $(\text{hy} + 4\text{Q} - \text{ne})/(\text{hy} + \text{di} + 4\text{Q} + \text{ne})$ is an index of silica saturation based on the basalts' normative mineralogy (5, 16).

K. W. W. Sims, Center for Isotope Geochemistry, Department of Geology and Geophysics, University of California, Berkeley, CA 94720, USA, and Los Alamos National Laboratory, Los Alamos, NM 87545, USA.

D. J. DePaolo, Center for Isotope Geochemistry, Department of Geology and Geophysics, University of California, Lawrence Berkeley Laboratory, Berkeley, CA 94720, USA.

M. T. Murrell, W. S. Baldrige, S. J. Goldstein, Los Alamos National Laboratory, Los Alamos, NM 87545, USA.

D. A. Clague, Hawaiian Volcano Observatory, Hawaii National Park, HI 96718, USA.

*To whom correspondence should be addressed.

Table 1. Sample locations, Sm and Nd concentrations, and Nd and Sr isotopes.

Sample	Location*	Sm (ppm)†	Nd (ppm)†	¹⁴⁷ Sm/ ¹⁴⁴ Nd‡	ε _{Nd} §	⁸⁷ Sr/ ⁸⁶ Sr
<i>Hawaiian basalts</i>						
KI-01-KWWS-92	Kilauea-Pu'u O'o	5.33	19.87	0.1622	6.1	0.70359
KL-F91-31	Kilauea-Pu'u O'o¶	4.38	16.45	0.1611	6.4	0.70355
ML-61-KWWS-92	Mauna Loa-Saddle Rd.	4.79	16.67	0.1737	4.4	0.70380
HU-05-KWWS-92	Hualalai-Hue Hue flow	5.04	22.13	0.1379	5.2	0.70360
HU-24-KWWS-92	Hualalai-Kaupulehu flow	5.12	22.78	0.1359	5.7	0.70357
MK-06-KWWS-92	Mauna Kea-Kalaleha flow	14.16	66.18	0.1294	7.1	0.70345
HK-02-KWWS-92	Haleakala-Kalua O Lapa flow	8.08	37.84	0.1291	7.7	0.70325
HK-06-KWWS-92	Haleakala-Luepalani flow	8.72	40.53	0.1301	8.3	0.70310
HK-11-KWWS-92	Haleakala-Pimoe flow	10.57	49.01	0.1305	8.2	0.70310
KK-19-1(WR)	Loihi	4.26	16.72	0.1541	4.9	0.70357
KK-19-1(GI)	Loihi	4.29	16.84	0.1541	5.0	0.70355
KK-27-14	Loihi	3.65	15.71	0.1405	5.5	0.70347
D8-1	South Arch	3.71	15.46	0.1450	6.8	0.70329
D9-11(WR)	South Arch	4.26	18.11	0.1423	7.6	0.70325
D9-11(GI)	South Arch	4.26	18.87	0.1367	7.2	0.70324
<i>MORBs</i>						
KK83-NP-124	Gorda Ridge, northern segment	3.54	10.53	0.2030	10.4	0.70239
KK83-NP-4-8	Gorda Ridge, northern segment	2.03	5.22	0.2350	11.9	0.70235
KK83-NP-6-16	Gorda Ridge, northern segment	5.21	15.63	0.2017	12.3	0.70242
All118-37	Juan de Fuca Ridge, Endeavour segment	2.33	6.85	0.2060	9.5	0.70240
TT175-17-23	Juan de Fuca Ridge, Endeavour segment	3.15	10.03	0.1896	9.7	0.70241
LII81WF-17	Juan de Fuca Ridge, southern segment	4.34	12.75	0.2060	10.3	0.70243

*Sample locations for: South Arch and Loihi (19); for MORBs (3). †Concentrations measured by ID-TIMS; measurement errors ≤0.4%. ‡Measurement errors (2σ) range from 0.1 to 0.2%. §¹⁴³Nd/¹⁴⁴Nd ratios, expressed in terms of ε_{Nd} (13), normalized to ¹⁴⁶Nd/¹⁴²Nd = 0.636151 and are relative to 0.511831 ± 17 for BCR-1 (our measured values at the Center for Isotope Geochemistry; measurement errors, based on in-run statistics, (2σ) ≤0.30 ε_{Nd} units. ||Measurement errors (2σ) ≤ 0.00002. ¶Collected from Pu'u O'o vent by Goff, 31 July 1991.

the correlations are consistent with simple models of trace-element fractionation during magma genesis (9, 10).

In the U/Th system, U/Th fractionation (denoted by *k_{U/Th}*) is determined from the disequilibrium activity ratio (²³⁸U/²³⁰Th)

measured in the lava. Because the 10⁵-year mean life of ²³⁰Th is not much larger than the time scale of magmatic processes, ²³⁰Th radioactive decay must be considered in the determination of U/Th fractionation from measured (²³⁸U/²³⁰Th) ratios (17). Both

the Hawaiian and MORB samples have activity ratios (²³⁸U/²³⁰Th) less than one (Fig. 2A and Table 2), indicating that Th was enriched in the melt relative to U during genesis of the basalts. Among the Hawaiian samples there is, with the exception of the

Table 2. Sample ages and U/Th concentrations and isotope ratios; the Th/U ratio is a weight ratio.

Sample *	Age (years)*	Th (ppm)†	U (ppm)†	Th/U	(²³⁰ Th/ ²³² Th)‡	(²³⁸ U/ ²³² Th)§	(²³⁸ U/ ²³⁰ Th)
<i>Hawaiian basalts</i>							
KL-1-KWWS-92	4	0.867	0.286	3.032	1.041	1.016	0.976
KL-F91-31	3	0.861	0.290	2.968	1.049	1.038	0.989
ML-61-KWWS-92¶	59	0.552	0.185	2.979	1.051	1.034	0.984
HU-05-KWWS-92	193	1.611	0.456	3.536	1.002	0.871	0.869
HU-24-KWWS-92	193	1.654	0.480	3.449	1.024	0.893	0.872
MK-06-KWWS-92	5630 ± 200	3.930	1.247	3.151	1.102	0.978	0.887
HK-02-KWWS-92	200	3.472	0.981	3.540	1.099	0.870	0.792
HK-06-KWWS-92	<1000	3.423	1.003	3.413	1.105	0.902	0.816
HK-11-KWWS-92	<1000	3.761	1.042	3.610	1.102	0.853	0.774
KK-19-19(wr)	500-1600	0.775	0.236	3.281	0.964	0.939	0.974
KK-19-1(gI)	500-1600	0.774	0.236	3.285	0.967	0.938	0.969
KK-27-14(wr)	500-1600	0.829	0.243	3.420	0.958	0.901	0.939
F288-HW D8-1(wr)	1000	0.936	0.281	3.325	0.936	0.926	0.989
F288 HW D9-11(wr)	1000	1.180	0.327	3.606	0.952	0.854	0.897
F288 HW D9-11(gI)	1000	1.127	0.312	3.607	0.947	0.854	0.902
<i>MORBs</i>							
KK83-NP-1-24	0 (axial)	0.278	0.091	3.050	1.249	0.995	0.796
KK83-NP-4-8	0 (axial)	0.037	0.015	2.390	1.304	1.269	0.974
KK83-NP-6-16	0 (axial)	0.334	0.111	3.011	1.232	1.008	0.818
All118-37	0 (axial)	0.322	0.103	3.140	1.327	0.966	0.728
TT175-17-23	0 (axial)	0.330	0.104	3.166	1.320	0.958	0.727
LII81WF-17	0 (axial)	0.273	0.112	2.456	1.413	1.239	0.877

*Radiometric and historic ages are from (19, 20); data and ages for MORBs have been reported in (3). †U and Th concentrations measured by isotope dilution-thermal ionization mass spectrometry (ID-TIMS), measurement errors in concentration ≤0.5%. ‡Denotes activity; λ₂₃₀ = 9.195 × 10⁻⁶ year⁻¹, λ₂₃₂ = 4.948 × 10⁻¹¹ year⁻¹; measured by high-abundance sensitivity-TIMS; errors (2σ) range from 0.4 to 0.6% for the Hawaiian basalts and from 0.5 to 1.0% for MORBs and do not include uncertainties in λ₂₃₀ (0.8%) or λ₂₃₂ (0.5%). §λ₂₃₈ = 1.551 × 10⁻¹⁰ year⁻¹; errors (2σ) do not include uncertainties in λ₂₃₈ (0.8%) or λ₂₃₂ and range from 0.4 to 0.5% for the Hawaiian basalts and from 0.5 to 0.9% for MORBs. ||Errors range from 0.6 to 0.8% for the Hawaiian basalts and from 0.7 to 1.6% for MORBs. ¶Results of an independent analysis on the same flow (32) agree within measurement error.

South Arch samples (18–21), a systematic relation between $k_{U/Th}$ and basalt type: tholeiitic basalts show the least U/Th fractionation ($k_{U/Th} = 0.98$ to 0.97); alkali basalts show an intermediate degree of fractionation ($k_{U/Th} = 0.94$ to 0.87); and basanites show the most U/Th fractionation ($k_{U/Th} = 0.79$ to 0.82). Correlations are also evident between $k_{U/Th}$ and $Na_{8.0}$ (Fig. 2B) and between $k_{U/Th}$ and the silica saturation index (Fig. 2C). These trends suggest that in the petrogenesis of Hawaiian basalts U/Th fractionation is systematically correlated with melt fraction (17). For the MORB samples the trends also show a systematic relation between $k_{U/Th}$ and their degree of trace-element enrichment: The N-MORBs have the higher $k_{U/Th}$ values (0.94 to 0.80), and the E-MORBs have lower $k_{U/Th}$ values (0.80 to 0.74). All of the MORB samples show significantly more U/Th fractionation than the Hawaiian tholeiites and, in some cases, more U/Th fractionation than the Hawaiian alkali basalts and basanites.

For the Hawaiian data there is a systematic relation between U/Th fractionation and Sm/Nd fractionation (Fig. 3), with Sm/Nd more fractionated than U/Th. The data can be inverted in terms of batch melting models to find self-consistent bulk U and Th partition coefficients and melt fractions. This inversion is based on the batch melting equation of Shaw (10), which is linear when expressed in terms of the parameters $(1 - \alpha_{Sm/Nd})^{-1}$ and $(1 - k_{U/Th})^{-1}$ (22). For the Hawaiian samples, regression of the $(1 - \alpha_{Sm/Nd})^{-1}$ and $(1 - k_{U/Th})^{-1}$ yields a slope of 26.25 ± 2.20 and an intercept of -53.25 ± 6.73 , with the correlation coefficient, r^2 , of 0.93. Assuming $D_{Nd} = 0.023$ and $D_{Sm} = 0.044$ (9), we calculate $D_U = 0.0014$ and $D_{Th} = 0.0006$; these values are similar to those calculated for a garnet lherzolite source ($D_U = 0.0012$ and $D_{Th} = 0.0003$) with the use of experimentally determined K_d values for garnet and clinopyroxene (12, 23, 24). The calculated melt fractions vary from a maximum of 6.5% for Hawaiian tholeiites to about 0.25% for basanites. Also shown in Fig. 3 is the batch melting trend for a spinel lherzolite source and both the batch and fractional melting (25) trends for a garnet lherzolite source; all are calculated with the experimentally determined values for D_U , D_{Th} , D_{Nd} , and D_{Sm} (26). The Hawaiian data agree with the batch melting trend for a garnet lherzolite source (12, 23, 24). As predicted, only samples that represent small melt fractions and have small $\alpha_{Sm/Nd}$ values show substantial U/Th fractionation. These observations imply that U/Th fractionation for Hawaiian basalts is a result of crystal-liquid fractionation occurring during partial melting in the presence of garnet.

The MORBs also show a significant cor-

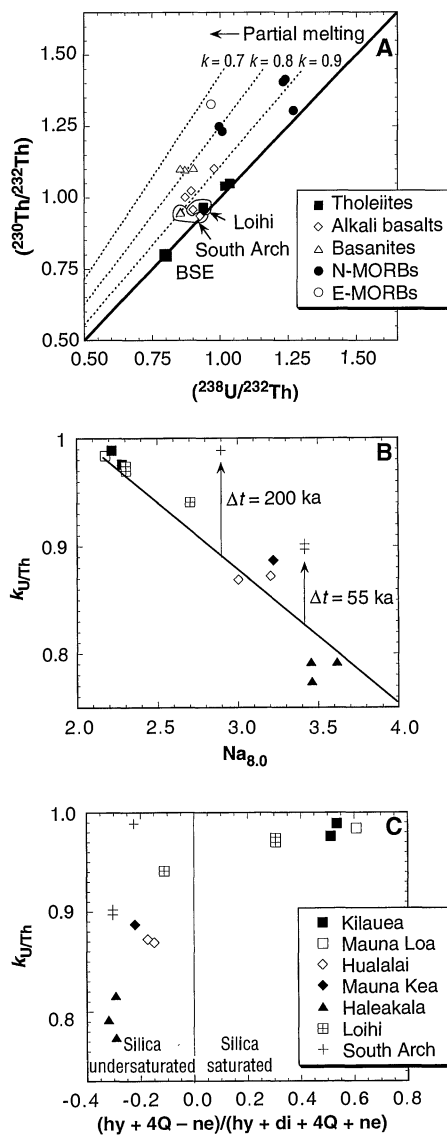


Fig. 2. (A) Plot of $(^{230}Th/^{232}Th)$ versus $(^{238}U/^{232}Th)$ for Hawaiian basalts and MORBs. The solid dark line is the equiline, representing the steady-state condition when the activity ratio of $(^{230}Th/^{232}Th)$ equals $(^{238}U/^{232}Th)$. If a mantle source has not been fractionated in the past 300,000 years, that source is constrained to lie along this equiline. Partial melting of a mantle source on this equiline produces a magma with a lower $(^{238}U/^{232}Th)$ but with the same $(^{230}Th/^{232}Th)$ value. The contours $k = 0.7, 0.8,$ and 0.9 represent lines of equal $^{238}U/^{232}Th$ fractionation relative to a mantle source on the equiline (17). The sizes of the data points are larger than the relative measurement error (2σ) based on in-run statistics (see Table 2). (B) Plot of $k_{U/Th}$ versus $Na_{8.0}$ for the Hawaiian basalts. For the South Arch samples the magnitude of the deviations from the indicated trend give model U/Th ages of ≈ 200 ka for the alkali basalt and ≈ 55 ka for the basanites (5, 16, 18). (C) Plot of $k_{U/Th}$ versus $(hy + 4Q - ne)/(hy + 4Q + ne)$ for the Hawaiian basalts.

relation between $k_{U/Th}$ and $\alpha_{Sm/Nd}$; the magnitude and the sign of the $k_{U/Th}$ values require partial melting in the presence of gar-

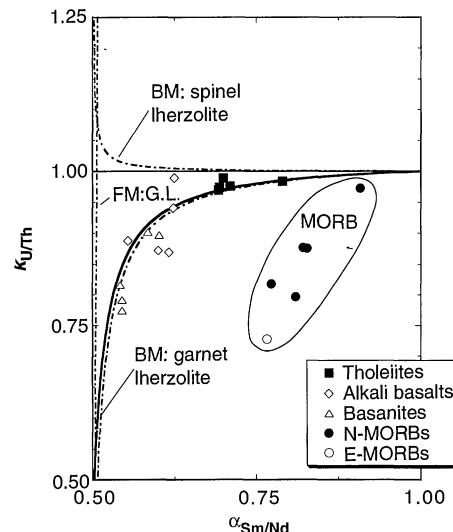


Fig. 3. Plot of $k_{U/Th}$ versus $\alpha_{Sm/Nd}$ for Hawaiian basalts and MORB samples. The dark solid line represents the batch melting trend inverted from the Hawaiian data (22). Also shown are the trends for batch melting of a spinel lherzolite source (BM: spinel lherzolite) and the batch (BM: garnet lherzolite) and fractional melting (FM: G.L.) of a garnet lherzolite source. Experimental partitioning data require that basalts lying in the lower half of this plot come from a source containing garnet. The batch and fractional melting trends represent end member models; other more complex melting models, such as dynamic melting, continuous melting, or the accumulated melt fraction from fractional melting, produce trends intermediate to these two trends. The sizes of the data points are larger than the propagated relative measurement errors (2σ).

net. In MORBs, however, $k_{U/Th} \approx \alpha_{Sm/Nd}$, a proportionality that is not easily reconciled with either batch or fractional melting models. The batch and fractional melting trends for a model garnet lherzolite source do not reproduce the observed trend of the MORB data (Fig. 3). Because these two models represent end-member models (27), dynamic melting and continuous melting also do not reproduce the MORB data. Explanations that would account for the MORB data fall into two categories. In the first, the model $\alpha_{Sm/Nd}$ values are valid and $k_{U/Th}$ is determined by (i) secondary processes not accounted for by mass balance melting models [for example, volatile exsolution, disequilibrium melting, fluid-melt interactions (7), and so on], (ii) some unknown phase that plays a significant role in fractionating U/Th and Sm/Nd and in which $D_{Nd} \approx D_{Th}$ and $D_{Sm} \approx D_U$, or (iii) mixing of melts of different melt fractions (5, 28). If the MORB data represent the mixing of different melt fractions, the almost one-to-one correlation between $k_{U/Th}$ and $\alpha_{Sm/Nd}$ requires that one of the end-member melt fractions be extremely small (melt fraction $F \approx 0.001$); for only near the limit of melting, when F is very small, is $k_{U/Th} \approx \alpha_{Sm/Nd}$. The mixing of

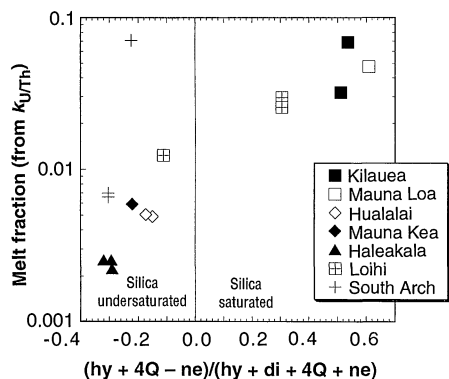


Fig. 4. Plot of melt fraction, derived from $k_{U/Th}$, versus $(hy + 4Q - ne)/(hy + di + 4Q + ne)$ for the Hawaiian basalts.

melts of different melt fractions is consistent with recent models that reproduce the chemistry and volume of MORBs by postulating a mixing of melts produced from a range of depths (5, 28). The second category of explanation is that the MORB source material does not conform to the model Sm/Nd value shown in Fig. 1A but rather has an $\alpha_{Sm/Nd}$ ratio $\sim 50\%$ higher than predicted by our chosen model (13). In this case, the MORB lavas would represent small melt fractions (approximately 0.2 to 2%) as suggested by McKenzie (4).

On the basis of our choice of D_{Sm} and D_{Nd} (29) and the observed U/Th fractionation for the Hawaiian samples, we calculate melt fractions of 2 to 6.5% for tholeiitic basalt, 0.5 to 1% for alkali basalt, and about 0.25% for basanite (Fig. 4). Melt fraction values for tholeiites from 5 to 7% are compatible with those suggested for Hawaiian basalts on the basis of fluid dynamical models (30, 31). However, 5 to 7% melt fractions for tholeiites and lesser values for more alkalic magmas are at the low end of the range of estimates based on high-pressure experimental phase equilibria studies: 5 to 35% for tholeiitic basalt, 10 to 20% for alkali basalt, and 1 to 15% for basanite (6). The discrepancy between melt fraction estimates based on trace-element fractionation and those based on experimental petrology could stem from complexities in the melting process, particularly for MORBs, as is illustrated by the combined U/Th and Sm/Nd data. On the other hand, for the Hawaiian samples, the consistency of the isotopic and major- and trace-element data and the agreement between our calculated melting trend and that predicted by experimentally measured K_d values lead us to favor the lower melt fraction estimates.

REFERENCES AND NOTES

1. M. Ivanovich and R. S. Harmon, Eds., *Uranium Series Disequilibrium: Applications to Environmental Problems* (Clarendon, Oxford, 1993); C. J. Allegre and

M. Condomines, *Nature* **299**, 21 (1982).
 2. M. Condomines, P. Morand, C. J. Allegre, *Earth Planet. Sci. Lett.* **55**, 247 (1981); S. Newman, R. C. Finkel, J. D. McDougall, *ibid.* **65**, 17 (1983); K. H. Rubin and J. D. McDougall, *ibid.* **114**, 149 (1992).
 3. S. J. Goldstein *et al.*, *ibid.* **96**, 134 (1989); S. J. Goldstein *et al.*, *ibid.* **109**, 255 (1992); S. J. Goldstein, M. T. Murrell, R. W. Williams, *ibid.* **115**, 151 (1993).
 4. D. McKenzie, *ibid.* **72**, 149 (1985).
 5. E. M. Klein and C. H. Langmuir, *J. Geophys. Res.* **92**, 8089 (1987); *ibid.* **94**, 4241 (1989).
 6. D. H. Green and A. E. Ringwood, *Contrib. Mineral. Petrol.* **15**, 103 (1967); D. H. Green, *Trans. Leicester Lit. Philos. Soc.* **44**, 26 (1970); B. O. Mysen and I. Kushiro, *Am. Mineral.* **62**, 843 (1977); A. D. Edgar, in *Alkaline Igneous Rocks*, J. G. Fitton and B. G. J. Upton, Eds. (Special Bulletin 30, Geological Society, London, 1987), p. 29.
 7. I. Reinitz and K. K. Turekian, *Geophys. Res. Lett.* **18**, 589 (1991); Z. Qin, *Geochim. Cosmochim. Acta* **57**, 1629 (1993).
 8. G. A. MacDonald and T. Katsura, *J. Petrol.* **5**, 82 (1964); M. D. Feigenson and F. J. Spera, *Geology* **9**, 531 (1981); M. D. Feigenson, A. W. Hofmann, F. J. Spera, *Contrib. Mineral. Petrol.* **84**, 390 (1983); C.-Y. Chen and F. A. Frey, *J. Geophys. Res.* **90**, 8743 (1985); F. A. Frey *et al.*, *ibid.* **95**, 1271 (1990).
 9. The "fractionation" of two elements (for example, Sm and Nd) caused by partial melting of mantle rock is related to melt fraction (F) by:

$$\alpha_{Sm/Nd} = \frac{Sm/Nd_{magma}}{Sm/Nd_{source}} = \frac{F + (1 - F)D_{Nd}}{F + (1 - F)D_{Sm}} \quad (1)$$
 where Sm/Nd_{magma} is determined from measurement of lava, Sm/Nd_{source} is the ratio in the mantle rock before melting, and D_{Nd} and D_{Sm} are solid-liquid chemical partition coefficients that depend on the mineralogy of the mantle "source" rock. Equation 1 applies to a simplified equilibrium model of the melting process (batch melting) (10) but also to more complicated melt percolation models if a steady state is maintained in the melting region (11). Note that $\alpha_{Sm/Nd}$ tends to unity, when F is much larger than D_{Nd} and D_{Sm} , indicating little Sm/Nd fractionation. The experimental D values for a source rock composed of the minerals olivine, orthopyroxene, clinopyroxene, and garnet are $D_{Nd} = 0.023$ and $D_{Sm} = 0.044$ (12). Maximum fractionation occurs for $F = 0$, whereupon $\alpha_{Sm/Nd} = D_{Nd}/D_{Sm} = 0.52$.
 10. D. M. Shaw, *Geochim. Cosmochim. Acta* **34**, 237 (1970).
 11. M. Spiegelman and P. Kenyon, *Earth Planet. Sci. Lett.* **109**, 611 (1992).
 12. J. G. Arth, *J. Res. U.S. Geol. Surv.* **4**, 41 (1976); G. A. McKay, in *Geochemistry and Mineralogy of Rare Earth Elements*, B. R. Lipin and G. A. McKay, Eds. (Reviews in Mineralogy, Mineralogical Society of America, Washington, DC, 1989), vol. 21, pp. 45-97.
 13. For most trace elements ratios, it is difficult to quantify the amount of chemical fractionation occurring during basalt petrogenesis because the ratio in the magma source is not known. However, for trace element ratios that are part of an isotopic system, such as Sm/Nd, Lu/Hf, and U/Th, isotopic abundances can be used to constrain the elemental ratio in the magma source (1, 14, 15). The model value for Sm/Nd_{source} is calculated from the measured $^{143}Nd/^{144}Nd$ of the lava (expressed as ϵ_{Nd}) using (14):

$$(^{147}Sm/^{144}Nd)_{source} = 0.195 \left(1 + \frac{\epsilon_{Nd}}{42.7} \right) \quad (2)$$

where

$$\epsilon_{Nd} = \left[\frac{(^{143}Nd/^{144}Nd)_{sample}}{0.511836} - 1 \right] \times 10^4 \quad (3)$$

Equation 3 (graphed in Fig. 1A) represents a 1.7×10^9 years ago (Ga) isochron through depleted mantle reservoir (DMR), average continental crust (not shown), and chondritic (CHUR) materials. The mantle is likely to be a mixture of these components; all mixtures will fall on one line. Small changes in the slope of the model line will not significantly affect the result.

14. D. J. DePaolo, *Nd Isotope Geochemistry: An Introduction* (Springer-Verlag, New York, 1988).

15. V. J. M. Salters and S. R. Hart, *Nature* **342**, 420 (1989).
 16. The index Na_{80} (5) accounts for the chemical effects of shallow crystallization by normalizing measured Na_2O content to a common reference value at 8% (by weight) MgO. Because Na behaves as an incompatible element during basalt petrogenesis, basalts resulting from smaller melt fractions have higher Na_{80} values. The "silica saturation index" is expressed in terms of normative minerals: $(hy + 4Q - ne)/(hy + di + 4Q + ne)$, where hy is hypersthene, Q is quartz, ne is nepheline, and di is diopside. Tholeiitic basalts have silica saturation indices greater than 1, whereas alkali basalts and basanites have indices less than 1.
 17. For U/Th an analogous formulation is used; the fractionation factor is denoted $k_{U/Th}$:

$$k_{U/Th} = \frac{U/Th_{magma}}{U/Th_{source}} = \frac{F + (1 - F)D_{Th}}{F + (1 - F)D_U} \quad (4)$$

U/Th_{source} is calculated from the $^{230}Th/^{232}Th$ (the ratio measured for the lava) by:

$$U/Th_{source} = \left[\frac{\lambda_{230}}{\lambda_{238}} \right] \left[\frac{^{230}Th}{^{232}Th} \right]_{lava} [exp \lambda_{230}(t + \Delta t_m)] - \left[\frac{^{238}U}{^{232}Th} \right]_{lava} [exp \lambda_{230}(t + \Delta t_m) - 1] \quad (5)$$

where λ_{230} ($9.195 \times 10^{-6} \text{ year}^{-1}$) and λ_{238} ($1.551 \times 10^{-10} \text{ year}^{-1}$) are the radioactive decay constants for ^{230}Th and ^{238}U , respectively, t is the time since eruption of the lava, and Δt_m is the time delay between formation of the magma in the mantle and eruption. For the U/Th system, the fractionation factor can be confidently estimated only if $\lambda_{230}(t + \Delta t_m) \ll 1$. For our samples, t is known; it is effectively zero for historic lavas and $\leq 0.05/\lambda_{230}$ (that is, ≤ 5000 years) for the other samples. For most of the samples we believe that $\Delta t_m \approx 0$, because the high MgO contents, relatively high Ni and Cr contents, and in some cases the presence of mantle xenoliths preclude long residence in a magma chamber. The Mauna Kea sample (a hawaiite) is an exception; it is petrologically evolved and could have Δt_m significantly greater than zero.

18. Deviation of the South Arch data from observed trends could be due to problems with the age assignments, estimated storage times, or fractionation caused by a volatile phase during melting. Ages used in Eq. 5 for the South Arch and Loihi samples were inferred from measured thicknesses of palagonite rinds (19); other prehistoric samples were radiocarbon-dated (20). South Arch samples deviate from the trends as if their true ages were 55×10^3 to 200×10^3 years older than their given ages, or their parental magmas had residence times of 55×10^3 to 200×10^3 years (Fig. 2B). The latter explanation is unlikely because the samples have high MgO, Ni, and Cr contents. Although it is conceivable that the ages from measured palagonite rind thicknesses are incorrect, qualitative observations suggest that the South Arch samples appear younger than those from Loihi, which do not exhibit similar offsets. If the observed deviations are not a result of incorrect age assignments, a more complex melting process must be invoked [for example, the involvement of a fluid phase in the melting process (21)].
 19. P. Lipman *et al.*, *Geology* **17**, 611 (1989); J. G. Moore, D. A. Clague, W. R. Normak, *ibid.* **10**, 88 (1982).
 20. S. C. Porter, *Geol. Soc. Am. Bull.* **90**, 980 (1979); R. B. Moore and D. A. Clague, *U.S. Geol. Surv. Map I-2213* (1991); D. R. Crandell, *U.S. Geol. Surv. Map I-1442* (1983).
 21. D. A. Clague and J. E. Dixon, *Eos* **72**, 563 (1991); paper presented at the International Workshop on Intraplate Volcanism, Tahiti, 2 August 1993.
 22. The batch melting equation can be written in the linear form as:

$$(1 - k_{U/Th})^{-1} = \left[\frac{(D_{Sm} - D_{Nd})}{(D_U - D_{Th})} \right] (1 - \alpha_{Sm/Nd})^{-1} + \left[\frac{-(D_{Sm} - D_U)}{(D_U - D_{Th})} \right] \quad (6)$$

A least squares linear fit of the data in the space of $(1 - \alpha_{Sm/Nd})^{-1}$ versus $(1 - k_{U/Th})^{-1}$ yields values for the two expressions in brackets. Given D_{Sm} and D_{Nd} , D_U and D_{Th} are uniquely determined and F can be calculated from Eqs. 1 and 4.

23. T. Z. La Tourrette and D. S. Burnett, *Earth Planet. Sci. Lett.* **110**, 227 (1992).
 24. P. Beattie, *Nature* **363**, 63 (1993); *Earth Planet. Sci. Lett.* **117**, 379 (1993).
 25. For modal melting, the concentration of an element in the liquid (C_A^L) produced by fractional melting (that is, perfect Rayleigh distillation) at a given F is given by (10):

$$C_A^L = \frac{C_A^0}{D_A} (1 - F)^{(1/D_A - 1)} \quad (7)$$

where C_A^0 is the concentration in the original source and D_A is the bulk partition coefficient. As with batch melting (for example, Eqs. 1 and 4), $k_{U/Th}$ and $\alpha_{Sm/Nd}$ can be expressed in terms of the ratio of two fractional melting equations.

26. The mineral weight fractions used for spinel lherzolite are as follows: olivine, 59%; orthopyroxene, 21%; clinopyroxene, 8%; and spinel, 12%; those used for garnet lherzolite are: olivine, 59%; orthopyroxene, 21%; clinopyroxene, 8%; and garnet, 12%. This yields for a spinel lherzolite source: $D_U = 7.2 \times 10^{-5}$, $D_{Th} = 1.04 \times 10^{-4}$, $D_{Nd} = 0.014$, and $D_{Sm} = 0.022$. For a garnet lherzolite source the values are: $D_U = 1.2 \times 10^{-3}$, $D_{Th} = 3.0 \times 10^{-4}$, $D_{Nd} = 0.023$, and $D_{Sm} = 0.044$ (12, 23, 24).

27. R. W. Williams and J. B. Gill, *Geochim. Cosmochim. Acta* **53**, 1607 (1989).
 28. E. R. Oxburgh, in *Physics of Magmatic Processes*, R. B. Hargraves, Ed. (Princeton Univ. Press, Princeton, NJ, 1980), pp. 161-199; M. Spiegelman and D. McKenzie, *Earth Planet. Sci. Lett.* **83**, 137 (1987); D. McKenzie and M. J. Bickle, *J. Petrol.* **29**, 625 (1988).
 29. Estimates of D_U , D_{Th} , and F , from our correlation of batch melting equations, depend on the selected values of D_{Sm} and D_{Nd} , which in our models are assumed to be constant. Changing the D_{Nd} and D_{Sm} values by $\pm 20\%$ would change the calculated F value by $\pm 50\%$ and the calculated D_U and D_{Th} by $\pm 3 \times 10^{-5}$ and $\pm 5 \times 10^{-5}$, respectively.
 30. S. Watson and D. McKenzie, *J. Petrol.* **32**, 501 (1991).
 31. N. M. Ribe, *Earth Planet. Sci. Lett.* **88**, 37 (1988).
 32. A. S. Cohen and R. K. O'Nions, *ibid.* **120**, 169 (1993).
 33. K.W.W.S. thanks E. Sklar, I. Carmichael, R. Jeanloz, and D. Pickett for valuable discussions pertaining to this project and T. Owens, D. Rokop, and P. Dixon for advice on matters pertaining to mass spectrometry. We also thank the anonymous reviewers. Support for this research was provided by grants from the Institute of Geophysics and Planetary Physics at Los Alamos National Laboratory, from Basic Energy Science, U.S. Department of Energy, and from the National Science Foundation (grant EAR93-04419).

17 August 1994; accepted 17 November 1994

Structural Basis for Sugar Translocation Through Maltoporin Channels at 3.1 Å Resolution

Tilman Schirmer,* Thomas A. Keller,† Yan-Fei Wang, Jurg P. Rosenbusch

Trimeric maltoporin (LamB protein) facilitates the diffusion of maltodextrins across the outer membrane of Gram-negative bacteria. The crystal structure of maltoporin from *Escherichia coli*, determined to a resolution of 3.1 angstroms, reveals an 18-stranded, antiparallel β -barrel that forms the framework of the channel. Three inwardly folded loops contribute to a constriction about halfway through the channel. Six contingent aromatic residues line the channel and form a path from the vestibule to the periplasmic outlet. Soaking of a crystal with maltotriose revealed binding of the sugar to this hydrophobic track across the constriction, which suggests that maltose and linear oligosaccharides may be translocated across the membrane by guided diffusion along this path.

Maltoporin (1), originally discovered as the receptor of bacteriophage λ (2), forms three water-filled channels across the outer membrane of Gram-negative bacteria (3). The maltoporin gene *lamB* (4) is part of the maltose regulon (5), which encodes the other proteins required for uptake and metabolism of maltose and linear maltooligosaccharides. For maltoporin, a sugar binding site with a dissociation constant of 10^{-4} M has been postulated (6, 7).

Crystals of maltoporin from *E. coli* con-

taining one trimer in the asymmetric unit (Table 1) were obtained as described (8). The structure was solved by a native Patterson correlation method (9), yielding the position of the local triad, followed by molecular averaging. After phase extension from 8 to 3.1 Å resolution, the resulting map was of high quality and allowed the entire polypeptide chain of 421 residues to be traced. The model has been partially refined with strict noncrystallographic symmetry constraints (10).

The scaffold of the monomer (Fig. 1) is an 18-stranded antiparallel β barrel forming a channel. Strands are connected to their nearest neighbors by long loops and turns. The loops are found at the end of the barrel that is exposed to the cell exterior. Three of them (L1, L3, and L6; Fig. 1) fold into the barrel and are, togeth-

er with loop L2 from an adjacent subunit, packed against the inner wall of the barrel and line the channel. The remaining loops form a compact structure at the cell surface.

Subunit interactions within the stable trimer structure (Fig. 2) involve peripheral contacts between L1 and L5, in addition to large parts of the barrel and loop L2 close to the molecular symmetry axis. A hydrophobic area encircles the trimer laterally and would match the core of the membrane in vivo. It is formed predominantly by short aliphatic residues. Eleven of those 14 transmembrane β strands that contribute to this area are flanked by aromatic residues at the nonpolar-polar boundary. Three polar residues, Asn²²⁸, Asp²⁷⁴, and Tyr²⁸⁸, are also located within the hydrophobic zone. Their compatibility with the environment of low dielectric constant is likely due to saturation of their hydrogen-bonding potential by mutual interactions. Resemblance of the maltoporin fold to that of nonspecific porins is obvious, although there is no detectable sequence homology, and nonspecific porins are about 80 residues shorter and form 16-stranded barrels with a single internal



Fig. 1. Schematic drawing of the maltoporin monomer. The cell exterior is at the top and the periplasmic space is at the bottom. The area of the subunit involved in trimer contacts is facing the viewer. The 18 antiparallel β strands of the barrel [shear number (24) = 22] are represented by arrows. Strands are connected to their nearest neighbors by loops or regular turns (25). Loops L1 (blue), L3 (red), and L6 (green) fold inward toward the barrel (see also Fig. 3A). L3 (red) is the major determinant of the constriction site. The yellow bond symbolizes the disulfide bridge Cys²²-Cys³⁸ within L1. Loop L2 (facing the viewer) latches onto an adjacent subunit in the trimer. Loops L4 to L6 and L9 form a large protrusion. The horizontal lines delineate the boundaries of the hydrophobic core of the membrane as inferred from the hydrophobic area found on the molecular surface. All figures were prepared with the program O (23).

T. Schirmer, Department of Structural Biology, Biozentrum, University of Basel, CH-4056 Basel, Switzerland.
 T. A. Keller, Y.-F. Wang, J. P. Rosenbusch, Department of Microbiology, Biozentrum, University of Basel, CH-4056 Basel, Switzerland.

*To whom correspondence should be addressed.

†Present address: Ecole Polytechnique Fédérale, Institut de Chimie Physique, CH-1015 Lausanne, Switzerland.